Mist chemical vapor deposition of MoO_2 thin films

Yuya Matamura, Takumi Ikenoue, Masao Miyake*, and Tetsuji Hirato

Graduate School of Energy Science, Kyoto University, Yoshida-honmachi, Sakyo-ku, Kyoto 606-8501, Japan

Email: miyake.masao.4e@kyoto-u.ac.jp

Keywords: A3. Chemical vapor deposition processes, B1. Oxides, A3. Polycrystalline deposition, A1. Crystal morphology

1. Introduction

Monoclinic molybdenum dioxide (MoO_2) with tetravalent Mo, which exhibits excellent chemical stability as well as high electrical conductivity (~10^{-4} Ω cm), has been studied as an active material for secondary batteries and photocatalytic materials [1–4]. Recently, MoO_2 has also been studied as the capacitor electrode of next-generation dynamic random access memory devices and the back contact of $Cu_2ZnSnSe_4$ solar cells because of its large work function and high resistance to reductive atmosphere [5,6].

MoO_2 thin films are prepared by various methods. Physical vapor deposition processes such as pulsed laser deposition and sputtering can yield smooth and dense MoO_2 films with excellent electrical characteristics [7–9]. However, these processes require the use of a high vacuum system and, therefore, have the disadvantages of low productivity and high energy consumption. In contrast, chemical vapor deposition (CVD) can generally be carried out with relatively low energy consumption. However, the formation of a dense MoO_2 film by CVD has not been reported to date.

In this study, MoO_2 thin films were prepared by the mist CVD method [10–15]. This method, which is also referred to as aerosol-assisted CVD, is a variant of CVD, in which the precursors are supplied to the reactor in the form of a mist rather than as vapor. As a mist is used in this process, materials with low volatility can be chosen as precursors,

in contrast to the highly volatile and toxic precursors used in conventional CVD processes. Another advantage of this method is that films can be formed under atmospheric pressure, and thus, at a lower cost. The preparation of high-quality metal oxide films, e.g., Ga_2O_3 and ZnO films, with excellent electrical properties has been realized by mist CVD [16,17]. Ashraf et al. performed mist CVD of MoO_2 using polyoxometalates as the precursor [18], but only obtained rough, sparse, powdery MoO_2. However, dense oxide films with a flat surface of Ga_2O_3, NiO, Cu_2O, and $LiMn_2O_4$ have been obtained by mist CVD using metal acetylacetonates as the precursor [10,11,19,20]. Mist CVD of MoO_2 using metal acetylacetonates as the precursor has not been reported before. In this study, mist CVD was performed using bis(acetylacetonato)molybdenum(VI) dioxide as the precursor to obtain flat MoO_2 films. Optimal deposition conditions including the deposition temperature and the position of the substrate in the reactor were determined by examining the crystal phase, morphology, and electrical resistivity of the resulting films.

2. Experimental

2.1. Materials

The precursor solution was prepared by dissolving 0.65 g of bis(acetylacetonato) molybdenum (VI) dioxide ($MoO_2(acac)_2$; Wako) in 80 mL of methanol containing 0.1

wt.% water. The concentration of water in methanol (99.8%, Wako) was measured using a Karl Fischer coulometer (KEM Kyoto, MKC-610) and was adjusted to be 0.1 wt.% by the addition of distilled water. The precursor solution was stirred for 6 h in a sealed container in dark, and then used for mist CVD. Glass slides (Matsunami; 25 mm × 76 mm, thickness: 1.0–1.2 mm) and quartz plates (26 mm × 76 mm; thickness: 1.0 mm) were used as the substrate for the MoO_2 films. Prior to their use, the substrates were cleaned with acetone, distilled water, and isopropanol using an ultrasonic bath and dried by blowing air.

2.2 Mist CVD of MoO_2

A custom-built hot-wall mist CVD system (Fig. 1) was used for the deposition of MoO_2 films. The system consists of a unit for generating the precursor mist and a reactor unit for film deposition. The precursor solution was taken in a glass cylinder (ϕ 95 mm) with a plastic film (~10 μm in thickness) covering the bottom of the cylinder, and the cylinder containing the solution was placed in a water bath, underneath which three ultrasonic atomizers (HM-2412, Honda Electronics) were installed. The mist of the precursor solution was generated by the ultrasonic vibration of the atomizers. The generated mist particles were transported to the reactor unit by a carrier gas (N_2). Additional N_2 gas was flown between the mist generator unit and reactor to dilute the

precursor mist in the gas flow. In the reactor unit, the substrates were placed in a quartz tube with an inner diameter of 40 mm and heated by an electric tube furnace (ϕ 51 mm × 300 mm, ARF-50KC, Asahi Rika Seisakusyo). Films were formed on the substrates through thermal decomposition of the precursor mist. Three pieces of the substrates were placed in the quartz tube side-by-side to cover the distance of 4–27 cm from the furnace inlet. The furnace temperature was monitored with a thermocouple attached to the outer wall of the quartz tube at the central part of the furnace, and the furnace temperature was controlled at a constant level in the range of 400–550 °C.

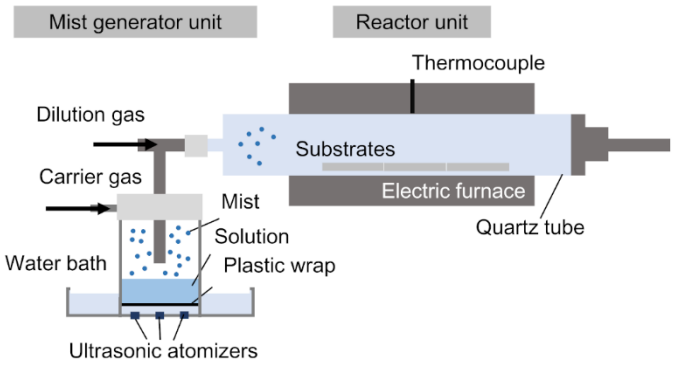

Fig. 1 Schematic illustration of a hot-wall mist CVD system.

The film deposition procedure is as follows: After placing the substrates in the quartz tube, the furnace was heated to a predetermined temperature and the quartz tube was purged with N_2. With the N_2 gas remaining in the furnace, the precursor solution was atomized for 5 min to stabilize the atomizers. Then, the carrier gas (N_2) and diluting

gas (N_2) were flown at the rates of 4 l and 2 l cm^3/min, respectively, and thus the mist was transported to the substrates in the furnace to start film deposition. After 10 min of film deposition, the carrier gas, atomizers, and furnace were turned off, while the flow of diluting gas was continued. Finally, the substrates were cooled to approximately room temperature (~ 25 °C) in the furnace under N_2 gas flow.

The temperature distribution on the substrate surface was measured under almost the same conditions as those during the film deposition, but a mist of methanol without $MoO_2(acac)_2$ was flown during this measurement. A thermocouple inserted from the end of the quartz tube was used to measure the temperature of the glass substrate surface. The temperature was recorded 10 min after the start of the mist flow. Direct measurement of substrate temperature was carried out at furnace temperatures of 350–480 °C, while the substrate temperatures at furnace temperatures of 500 and 550 °C were determined by extrapolation of the data collected at the lower furnace temperatures.

2.3. Characterization of films

X-ray diffraction (XRD) was performed with an X-ray diffractometer (X'pertPRO-MPD, PANalytical) using Cu-$K\alpha$ radiation to evaluate the phase of the deposited film. The morphology of the deposited film was observed by field emission scanning electron microscopy (SEM, JSM-6510LV, JEOL). The electrical resistivity was measured at room

temperature (~25 °C) by the four-probe method with an applied current of 10 μA using a source meter (2450 SourceMeter, KEITHLEY). The glass substrate after film deposition was cut into several pieces, and the resistivity of the film on each piece was measured to determine the distribution of the resistivity.

X-ray photoelectron spectroscopy (XPS) was performed on a JPS-9030 spectrometer (JEOL) using a Mg $K\alpha$ X-ray source (1253.6 eV) operated at 12.0 kV and 10.0 mA to analyze the oxidation state of elements present in the prepared films. The base pressure of the instrument was typically less than 5×10^{-6} Pa. The XPS spectra were calibrated using the C 1s peak from hydrocarbon contamination fixed at 285.0 eV. A pass energy of 50 eV with 1 eV step was used for collecting the wide-scan survey spectrum, while a pass energy of 30 eV with 0.2 and 0.05 eV step, respectively, was used for collecting the spectra in the C 1s and Mo 3d regions. Sputter etching of the samples was carried out using an argon ion gun operated at 400 V for 5 s with a duty ratio of 50%. Under the acceleration voltage of 400 V, a standard SiO_2 film is etched at the rate of approximately 0.3 nm s^{-1}. The XPS spectra were analyzed using SPECSURF (version 2.0.5.7, JEOL) software. The Mo 3d spectrum typically consists of two envelopes because of the consequence of spin-orbit coupling. The ratio of the oxidation states of Mo in specimens was estimated by the deconvolution of the spectra using a method suggested

by Choi et al. [21]. The Mo $3d_{5/2}$–Mo $3d_{3/2}$ doublet was fitted so that each peak had the same mixed Gaussian-Lorentzian line shape and width. The intensity ratio and the splitting energy for the Mo $3d_{5/2}$–Mo $3d_{2/3}$ doublet was fixed at $I(3d_{5/2})/I(3d_{5/2}) = 3/2$ and 3.15 eV, respectively. The XPS spectrum of the prepared film was compared with those of MoO_2 and MoO_3 powders. The MoO_2 powder (99.9%) was purchased from Kojundo Chemical Laboratory and the MoO_3 powder was prepared by annealing molybdenum metal powder (99.9%, Wako) in air at 500 °C for more than 8 h. These powders were confirmed to be single phases of monoclinic MoO_2 and orthogonal MoO_3 by XRD analysis.

3. Results and Discussion

The temperature of the substrate is one of the key factors that can greatly affect the quality of the resulting film in mist CVD. Figure 2 shows the temperature distributions over the substrate surface under the mist flow in the furnace heated to various preset temperatures in the range of 400–550 °C. At every furnace temperature, the temperature of the substrate surface was found to have a maximum value at a position slightly downstream from the center of the furnace. Without the mist flow, the maximum temperature is observed at the center, which is 15 cm from the inlet of the furnace. The

quality of the resulting film is likely to be affected not only by the substrate temperature but also by the time taken by the mist to travel through the heating zone to the substrate. Therefore, we examined the films formed at different positions in the furnace at various preset temperatures.

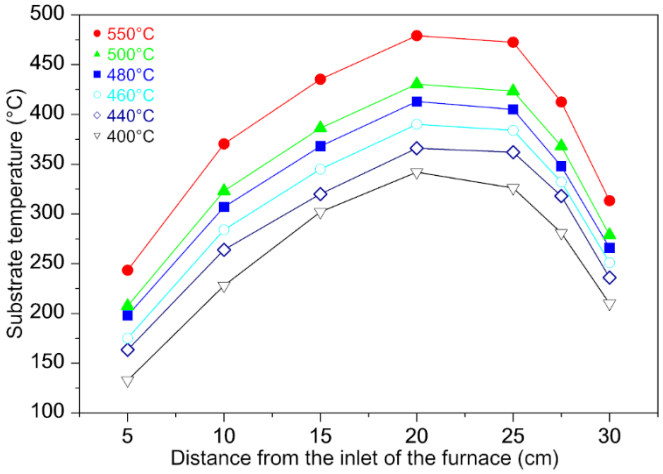

Fig. 2 Temperature distribution on the substrate under mist flow in the furnace at different preset temperatures.

Figure 3 shows the photographs of the films formed on the glass substrates by the mist CVD at furnace temperatures of 550 and 480 °C. Films were formed over a length of >14 cm on the substrates. The films obtained at the furnace temperature of 550 °C have a dull gray appearance near the center of the substrate and a dark reflective appearance near both ends. Meanwhile, the entire film obtained at the furnace temperature of 480 °C has a uniform reflective appearance.

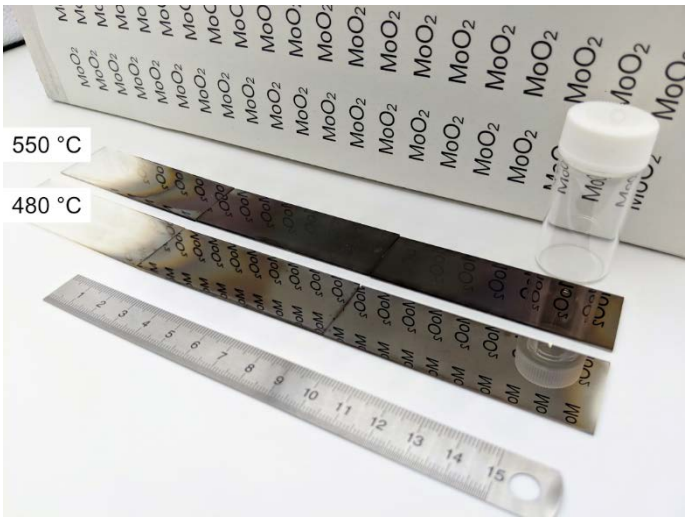

Fig. 3 Photographs of films prepared at furnace temperatures of 550 °C (top) and 480 °C (bottom). The mist was flown in from the left side of the substrate during the process.

Figure 4 schematizes the appearance of the films formed at different locations in the furnace at different temperatures. No film formation was observed at a furnace temperature of 400 °C. Film deposition occurred at furnace temperatures higher than 440 °C. At the furnace temperatures of 440–500 °C, films with metallic luster (see the photograph in Fig. 3) were obtained over a wide area, while at 550 °C, a dark mirror-like or grayish dull film was obtained.

At the furnace temperature of 440 °C, the film was formed in the range of X = 15 cm to 25 cm, where X is the distance from the inlet of the furnace (Fig. 4). The starting edge of the formed film shifted upstream as the furnace temperature was increased, and

thus, the area over which the film formed increased with increasing furnace temperature. A comparison between the temperature distribution (Fig. 2) and the starting edge of the formed film (Fig. 4) indicates that the film deposition started at the position where the substrate temperature is approximately 325 °C.

The characteristics of the films obtained at different furnace temperatures and the differences in the characteristics at different positions of a given film grown at a particular furnace temperature (the regions indicated by the circles in the diagram in Fig. 4) are discussed hereafter.

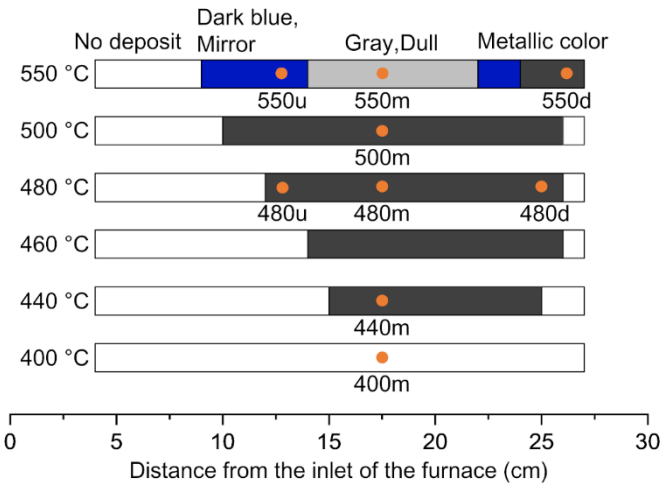

Fig. 4. Diagram showing the physical appearance of films deposited at different positions in a furnace at various temperatures. The circles indicate the positions of the films characterized intensively in this study.

Figure 5 shows the XRD patterns of the films obtained from the area near the

middle of the furnace (at X = 18 cm). The XRD pattern of the sample obtained at a furnace temperature of 400 °C showed only a halo from the glass substrate, confirming that no film deposition occurred at this temperature. In the XRD patterns for films prepared at 440 °C and 480 °C, peaks are observed at 2θ = 36.6°, 52.8°, 36.9°, and 53.2°. These peaks correspond to the crystal planes of monoclinic MoO_2 [22]. No diffraction peak was observed from the film at 2θ = 26°, where MoO_2 (011) diffraction peak should appear if the deposited film consists of randomly oriented grains. The film, therefore, appears to be composed of MoO_2 with a preferred orientation. The strong diffraction observed at 2θ = 37° can be attributed to either (2 0 −2), (2 1 −1), (0 2 0), or (0 0 2) plane of MoO_2. The diffraction peaks from these lattice planes are so close that it was impossible to uniquely identify the oriented lattice plane.

In the XRD patterns of the films prepared at 500 °C and 550 °C, the diffractions of MoO_2 and an additional phase were observed. The diffraction pattern from the additional phase corresponded to that of $K_2Mo_8O_{16}$ (ICSD Code: 060242).$K_2Mo_8O_{16}$ could be derived by the diffusion of K incorporated as an additive in the glass substrate into the growing film at high temperatures. This hypothesis was confirmed by the film deposited on a quartz substrate. On the quartz substrate, MoO_2 film without the $K_2Mo_8O_{16}$ phase was obtained at 550 °C (Fig. 6).The formation of $K_2Mo_8O_{16}$ can be

prevented by the use of the quartz substrate. However, at the furnace temperature of 550 °C, the deposited films on both quartz and glass were rough and not as smooth as the ones deposited at 480 °C, a temperature that is low enough to prevent the formation of the additional phase.

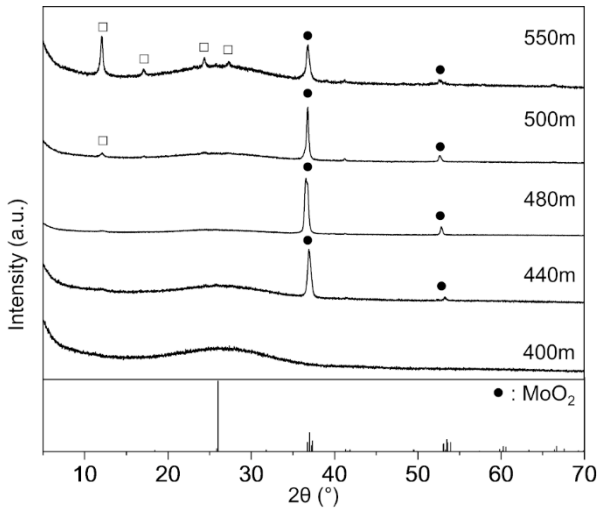

Fig. 5 XRD patterns of films deposited at a position of 18 cm away from the inlet of a furnace set at different temperatures (400–550 °C).

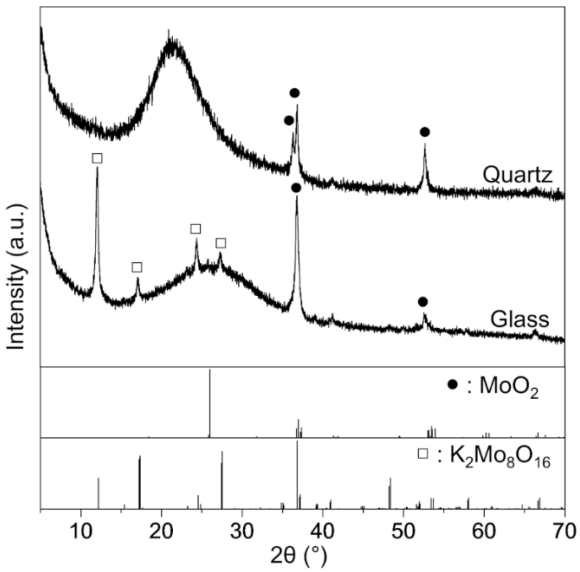

Fig. 6 XRD patterns of films deposited at 550 °C on quartz and glass substrates.

The films formed at different positions in the furnace at temperatures of 480 °C and 550 °C (indicated as 480u, 480m, 480d, 550u, 550m, and 550d in Fig. 4) were analyzed to examine the differences in the deposited phase according to the substrate position in the furnace. Figure 7 shows the XRD patterns of the films. At the furnace temperature of 480 °C, the single-phase MoO_2 film with the preferred orientation was obtained at every substrate position from upstream to downstream. The film obtained at the furnace temperature of 550 °C contained MoO_2 and $K_2Mo_8O_{16}$ at every position.

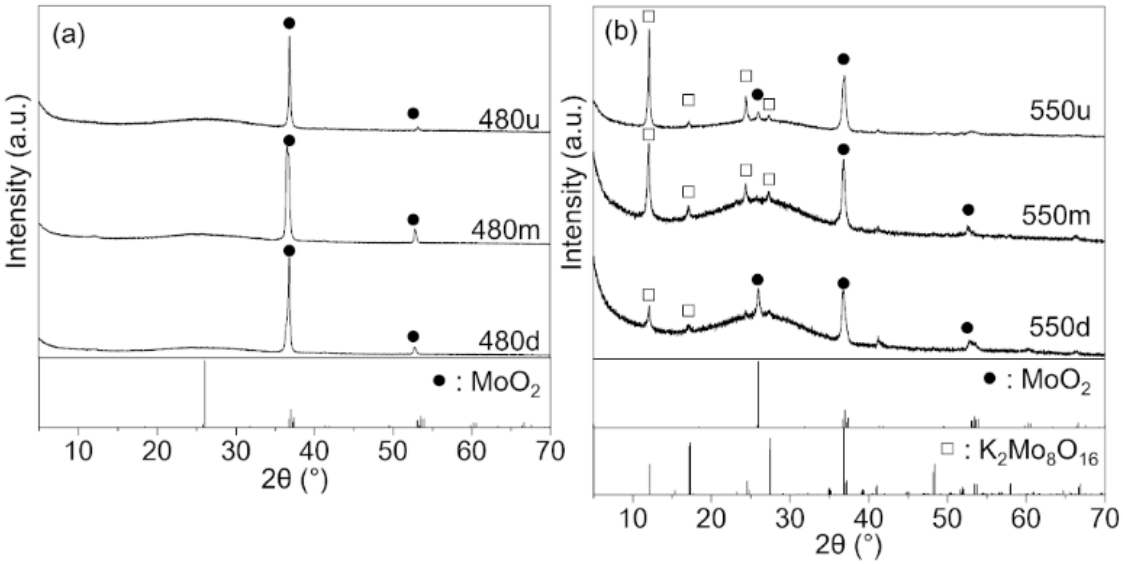

Fig. 7 XRD patterns of films deposited at various positions in a furnace set at temperatures of (a) 480 °C and (b) 550 °C.

The film formed at X = 18 cm in the furnace at 480 °C was further analyzed by XPS. For comparison, the XPS spectra of MoO_2 and MoO_3 powders were also acquired. Figure 8 shows the survey scan spectrum in the binding energy range of 0–1000 eV, where only the signals of molybdenum, oxygen, and carbon are observed. The signals of carbon from the film diminished to the noise level after Ar^+ ion etching, indicating that the carbon signal detected before etching originated from hydrocarbon contamination on the film surface and the film is essentially composed of molybdenum and oxygen only.

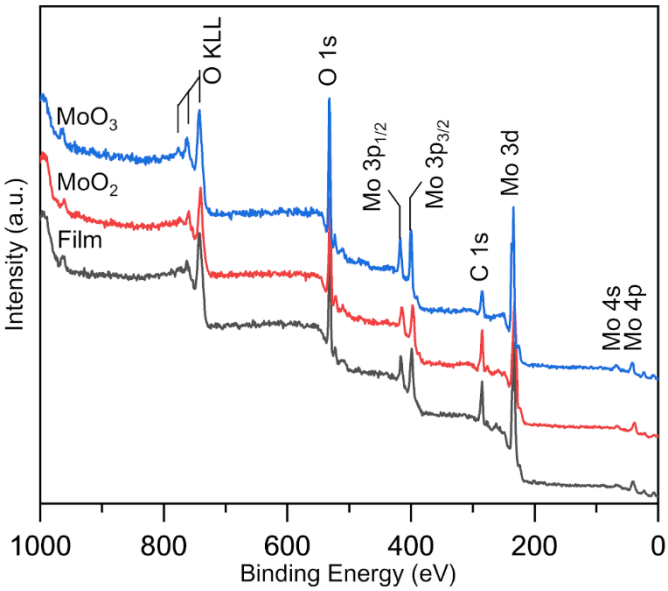

Fig. 8 Wide-scan XPS spectra of (a) a MoO_2 thin film prepared by mist CVD, (b) MoO_2 powder, and (c) MoO_3 powder.

Figure 9 shows the XPS spectra in the Mo 3d region. In the spectrum acquired before Ar^+ ion etching, Mo(V) is dominant on the surface of the prepared film. Note that

Mo(V) is dominant even in MoO_2 powder, while Mo(VI) is mostly detected from MoO_3 powder. The presence of Mo(V) in the MoO_2 powder should be because of surface oxidation. It is well known that the MoO_2 surface is easily oxidized [23,24]. After etching for 5 s, the signal of Mo(IV) was detected more significantly from the film as well as MoO_2 powder. The decrease in the Mo(V) signals can be attributed to the removal of the surface oxidation layer by Ar^+ ion etching as well as the reduction of some molybdenum to Mo(IV) due to Ar^+ ion bombardment. Comparison of the spectra of MoO_3 powder before and after etching indicates that Mo(VI) was reduced to Mo(V) by Ar^+ ion bombardment, but hardly to Mo(IV).

The similarity in the spectral features of the film and MoO_2 powder suggests that the film is composed of MoO_2, although there is a possibility that the average valence of Mo could be slightly higher in the film than in MoO_2. The possible reduction of Mo(V) to Mo(IV) by Ar^+ ion bombardment leaves this ambiguity in the analysis.

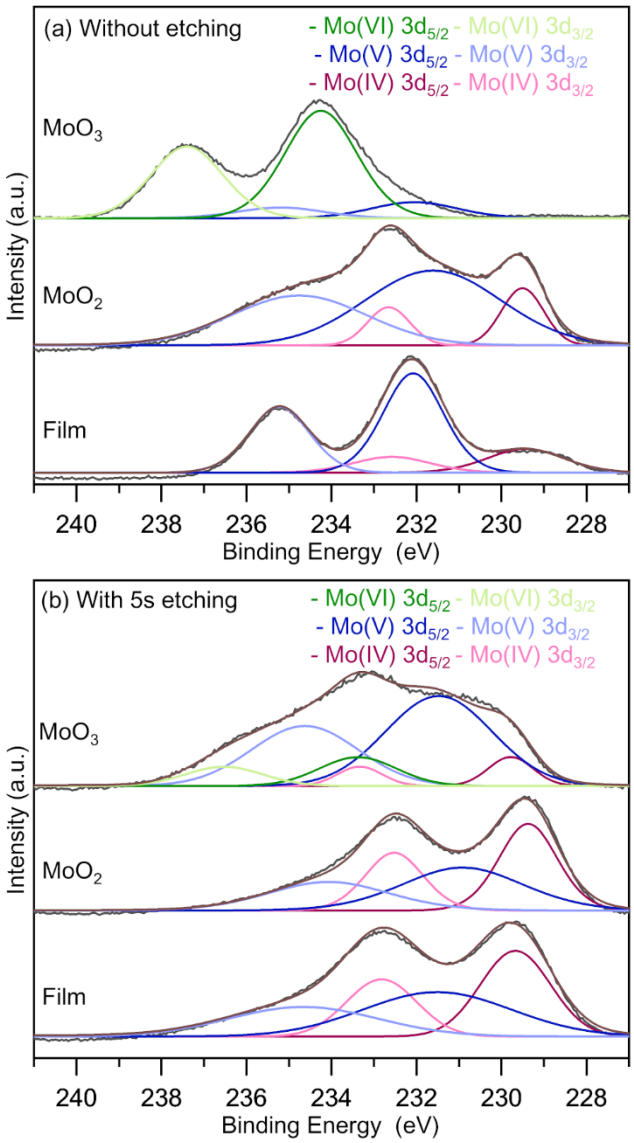

Fig. 9 Mo 3d spectra of a MoO_2 thin film prepared by mist CVD, MoO_2 powder, and MoO_3 powder (a) before and (b) after Ar^+ ion etching for 5 s.

Figure 10 shows the surface and cross-sectional SEM images of the films. Fig. 10 (a–c) shows that the film prepared at the furnace temperature of 550 °C is composed of sparsely deposited crystalline grains and its surface is rough, particularly at the

upstream and midstream areas. Fig. 10 (b,d–f) show that the films prepared at lower furnace temperatures are composed of fine crystalline grains that densely cover the substrate surface. The films prepared at the furnace temperatures of 480 and 440 °C are especially smooth and dense. The cross-sectional SEM images suggest that at 550 °C, new crystalline grains were generated constantly during the film growth, whereas at temperatures of 480 °C and 440 °C, after the nucleation of grains on the substrate, only their growth took place. At the furnace temperatures of 480 °C and 440 °C, the MoO_2 films were densely deposited and the entire film surface was smooth. This result indicates that smooth and dense MoO_2 films can be obtained over a wide area by mist CVD.

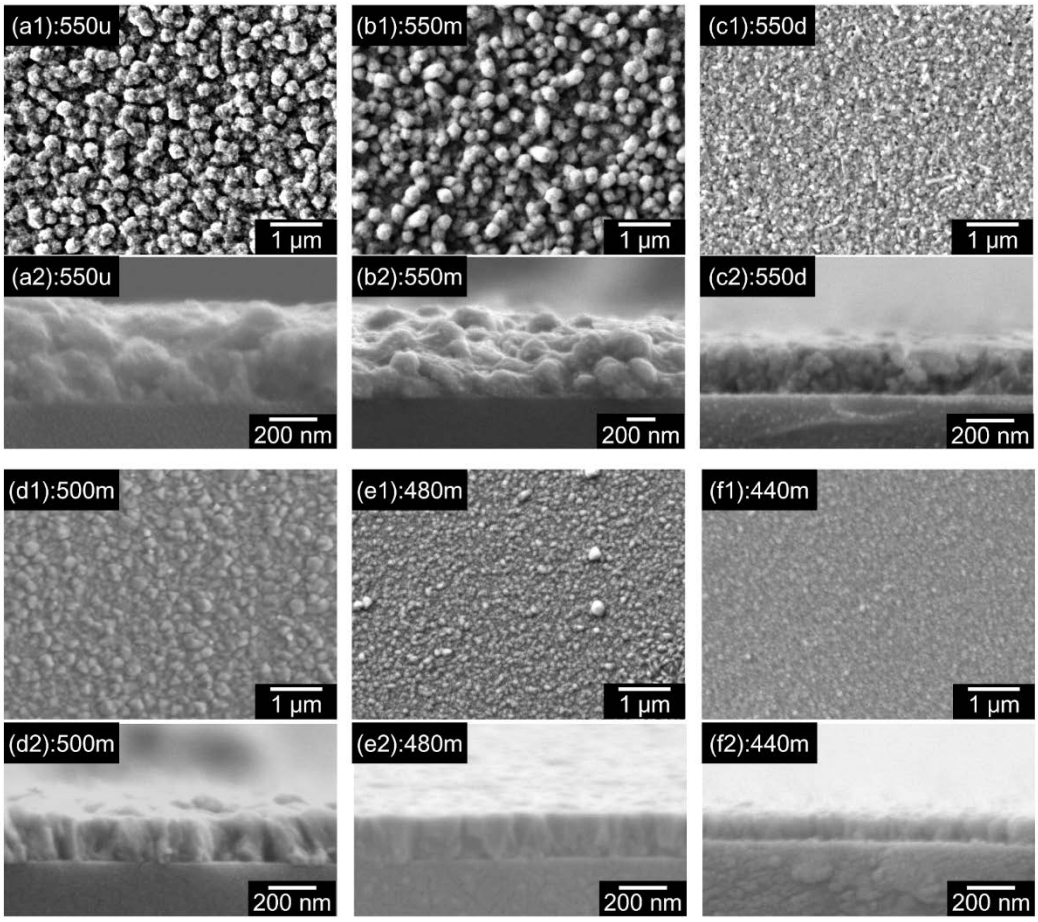

Fig. 10 Surface and cross-sectional SEM images of films prepared in a furnace at temperatures of 440–550 °C. (a, b, c) Films obtained at upper, middle, and downstream areas in the furnace at 550 °C. (d, e, f) Films obtained at the middle stream area in the furnace at 500, 480, and 440 °C.

Figure 11 shows the distribution of the film thickness determined from the cross-sectional SEM images. At the furnace temperatures of 500 °C and 480 °C, the film thickness was constant at ~200 nm in the range of ~15–23 cm from the furnace inlet.

The films prepared at a lower furnace temperature (440 °C) were relatively thinner, and the film was not uniform in any region. The film prepared at a high temperature of 550 °C was significantly thicker, but contained no uniform region.

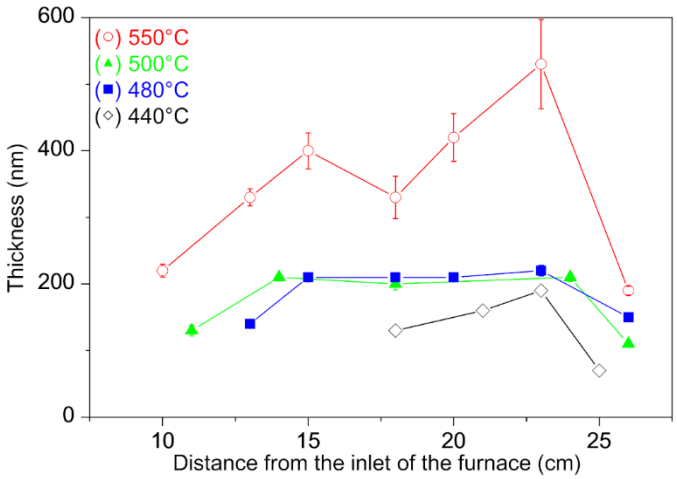

Fig. 11 Distribution of the thickness of films prepared at different furnace temperatures.

Figure 12 shows the electrical resistivity of the films. The films prepared at the furnace temperatures of 440–500 °C showed a low resistivity of the order of 10^{-3} Ω cm throughout the film. This resistivity is one order of magnitude higher than that of the MoO_2 film prepared by vacuum processes [5,7] (10^{-4} Ω cm), but one order of magnitude smaller than that of the MoO_2 prepared by a solution process [2] (10^{-2} Ω cm). The film prepared at 550 °C showed a relatively high resistivity of 10^{-2} Ω cm. The high resistivity can be attributed to the additional phase included in the film and the less dense morphology of the film.

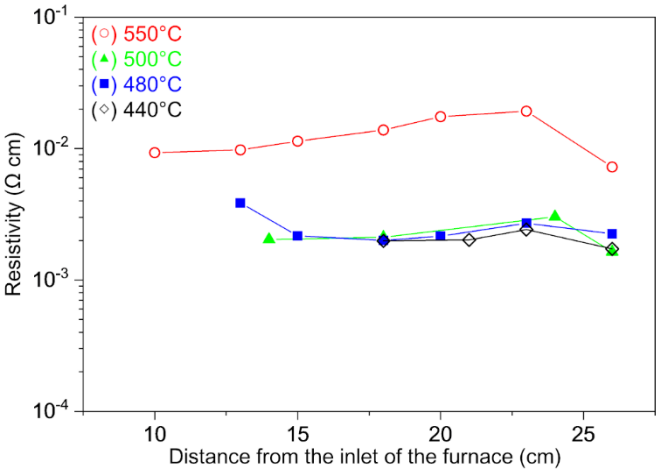

Fig. 12 Electrical resistivity of the MoO_2 film as a function of the distance from the inlet of the furnace at different preset temperatures.

In general, a CVD process includes the following four steps: (1) transport of precursors, (2) diffusion and adsorption of precursors to the substrate, (3) progress of the chemical reaction on the substrate surface, and (4) removal of byproducts. The rate-limiting step changes according to the temperature: it tends to be the chemical reaction on the substrate surface (step 3) at low temperatures and the diffusion/adsorption of precursors to the substrate (step 2) at high temperatures. When the temperature is increased further, solid particles are precipitated in the gas phase during the transportation (step 1) before the precursors reach the substrate.

In the present study, the thickness of the film deposited at the furnace temperature of 550 °C was significantly greater than that of the films obtained at lower temperatures.

As discussed previously, the SEM images of the film (Fig. 10) revealed that new crystal grains were generated during the film deposition at 550 °C. This result suggests that solid particles were precipitated in the gas phase during the transport of the mist and the precipitates settled on the growing film. In other words, at 550 °C, the precipitation of MoO_2 powder occurred concomitant with the crystal growth on the substrate by the chemical reaction of the precursor. At lower furnace temperatures of 500 °C and 480 °C, a uniformly thick film was formed over a wide area (Fig. 11), although the substrate temperature varied depending on the position of the substrate. Furthermore, as shown in Fig. 8, all the crystal grains appeared to have grown on the substrate at these temperatures. Therefore, the diffusion and adsorption of the precursor from the gas phase to the substrate (step 2) appears to be the rate-limiting step at these temperatures. At 440 °C, the film thickness varied depending on the substrate temperature, indicating that the chemical reaction on the surface is the rate-limiting step at this temperature.

4. Conclusions

We demonstrated that dense and smooth MoO_2 films can be obtained by mist CVD using acetylacetonate salt as the precursor. The MoO_2 films were deposited at furnace temperatures of ≥440 °C; however, an additional phase ($K_2Mo_8O_{16}$) was included for the

MoO_2 films deposited at a furnace temperature of 550 °C. Despite the temperature distribution over the substrate surface, a smooth MoO_2 film with a constant thickness of 200 nm was uniformly deposited over a wide area of the substrates at furnace temperatures in the range 480–500 °C. The prepared MoO_2 films showed a low resistivity of 2×10^{-3} Ω cm. This study provides a low-cost fabrication method for MoO_2 thin films.

Acknowledgments

This work was partly supported by KAKENHI (Grant No. 18K18943).

References

[1] D.B. Rogers, R.D. Shannon, A.W. Sleight, J.L. Gillson, Crystal chemistry of metal dioxides with rutile-related structures, Inorg. Chem. 8 (1969) 841–849. https://doi.org/10.1021/ic50074a029.

[2] Y. Shi, B. Guo, S.A. Corr, Q. Shi, Y.-S. Hu, K.R. Heier, L. Chen, R. Seshadri, G.D. Stucky, Ordered mesoporous metallic MoO_2 materials with highly reversible lithium storage capacity, Nano Lett. 9 (2009) 4215–4220. https://doi.org/10.1021/nl902423a.

[3] H. Choi, J.H. Heo, S. Ha, B.W. Kwon, S.P. Yoon, J. Han, W.-S. Kim, S.H. Im, J. Kim, Facile scalable synthesis of MoO_2 nanoparticles by new solvothermal cracking process and their application to hole transporting layer for $CH_3NH_3PbI_3$ planar perovskite solar cells, Chem. Eng. J. 310 (2017) 179–186. https://doi.org/10.1016/j.cej.2016.10.110.

[4] Y. Sun, X. Hu, W. Luo, Y. Huang, Self-assembled hierarchical MoO_2/graphene nanoarchitectures and their application as a high-performance anode material for lithium-ion batteries, ACS Nano. 5 (2011) 7100–7107. https://doi.org/10.1021/nn201802c.

[5] W. Lee, C.J. Cho, W.C. Lee, C.S. Hwang, R.P.H. Chang, S.K. Kim, MoO_2 as a

thermally stable oxide electrode for dynamic random-access memory capacitors, J. Mater. Chem. C. 6 (2018) 13250–13256. https://doi.org/10.1039/C8TC04167A.

[6] S. Lopez-Marino, M. Espíndola-Rodríguez, Y. Sánchez, X. Alcobé, F. Oliva, H. Xie, M. Neuschitzer, S. Giraldo, M. Placidi, R. Caballero, V. Izquierdo-Roca, A. Pérez-Rodríguez, E. Saucedo, The importance of back contact modification in $Cu_2ZnSnSe_4$ solar cells: The role of a thin MoO_2 layer, Nano Energy. 26 (2016) 708–721. https://doi.org/10.1016/j.nanoen.2016.06.034.

[7] V. Bhosle, A. Tiwari, J. Narayan, Epitaxial growth and properties of $MoO_x(2<x<2.75)$ films, J. Appl. Phys. 97 (2005) 083539. https://doi.org/10.1063/1.1868852.

[8] E. Ahn, Y.-S. Seo, J. Cho, I. Lee, J. Hwang, H. Jeen, Epitaxial growth and metallicity of rutile MoO_2 thin film, RSC Adv. 6 (2016) 60704–60708. https://doi.org/10.1039/C6RA09928A.

[9] C. Liu, Z. Li, Z. Zhang, MoO_x thin films deposited by magnetron sputtering as an anode for aqueous micro-supercapacitors, Sci. Technol. Adv. Mater. 14 (2013) 065005. https://doi.org/10.1088/1468-6996/14/6/065005.

[10] T. Ikenoue, S. Sakamoto, Y. Inui, Fabrication and characteristics of p-type Cu_2O

thin films by ultrasonic spray-assisted mist CVD method, Jpn. J. Appl. Phys. 53 (2014) 05FF06. https://doi.org/10.7567/JJAP.53.05FF06.

[11] D. Shinohara, S. Fujita, Heteroepitaxy of corundum-structured α-Ga_2O_3 thin films on α-Al_2O_3 substrates by ultrasonic mist chemical vapor deposition, Jpn. J. Appl. Phys. 47 (2008) 7311–7313. https://doi.org/10.1143/JJAP.47.7311.

[12] T. Kawaharamura, H. Nishinaka, S. Fujita, Growth of crystalline zinc oxide thin films by fine-channel-mist chemical vapor deposition, Jpn. J. Appl. Phys. 47 (2008) 4669–4675. https://doi.org/10.1143/JJAP.47.4669.

[13] H. Nishinaka, T. Kawaharamura, S. Fujita, Low-temperature growth of ZnO thin films by linear source ultrasonic spray chemical vapor deposition, Jpn. J. Appl. Phys. 46 (2007) 6811–6813. https://doi.org/10.1143/JJAP.46.6811.

[14] H. Ito, K. Kaneko, S. Fujita, Growth and band gap control of corundum-structured α-$(AlGa)_2O_3$ thin films on sapphire by spray-assisted mist chemical vapor deposition, Jpn. J. Appl. Phys. 51 (2012) 100207. https://doi.org/10.1143/JJAP.51.100207.

[15] T. Uchida, T. Kawaharamura, K. Shibayama, T. Hiramatsu, H. Orita, S. Fujita, Mist chemical vapor deposition of aluminum oxide thin films for rear surface passivation of crystalline silicon solar cells, Appl. Phys. Express. 7 (2014)

021303. https://doi.org/10.7567/APEX.7.021303.

[16] T. Kawaharamura, G.T. Dang, M. Furuta, Successful growth of conductive highly crystalline Sn-doped α-Ga_2O_3 thin films by fine-channel mist chemical vapor deposition, Jpn. J. Appl. Phys. 51 (2012) 040207. https://doi.org/10.1143/JJAP.51.040207.

[17] J.G. Lu, T. Kawaharamura, H. Nishinaka, Y. Kamada, T. Ohshima, S. Fujita, ZnO-based thin films synthesized by atmospheric pressure mist chemical vapor deposition, J. Cryst. Growth. 299 (2007) 1–10. https://doi.org/10.1016/j.jcrysgro.2006.10.251.

[18] S. Ashraf, C.S. Blackman, G. Hyett, I.P. Parkin, Aerosol assisted chemical vapour deposition of MoO_3 and MoO_2 thin films on glass from molybdenum polyoxometallate precursors; thermophoresis and gas phase nanoparticle formation, J. Mater. Chem. 16 (2006) 3575. https://doi.org/10.1039/b607335b.

[19] T. Ikenoue, J. Inoue, M. Miyake, T. Hirato, Epitaxial growth of undoped and Li-doped NiO thin films on α-Al_2O_3 substrates by mist chemical vapor deposition, J. Cryst. Growth. 507 (2019) 379–383. https://doi.org/10.1016/j.jcrysgro.2018.11.032.

[20] K. Tadanaga, A. Yamaguchi, A. Sakuda, A. Hayashi, M. Tatsumisago, A. Duran,

M. Aparacio, Preparation of $LiMn_2O_4$ cathode thin films for thin film lithium secondary batteries by a mist CVD process, Mater. Res. Bull. 53 (2014) 196–198. https://doi.org/10.1016/j.materresbull.2014.01.032.

[21] J.-G. Choi, L.T. Thompson, XPS study of as-prepared and reduced molybdenum oxides, Appl. Surf. Sci. 93 (1996) 143–149. https://doi.org/10.1016/0169-4332(95)00317-7.

[22] A. Bolzan, B. Kennedy, C. Howard, Neutron powder diffraction study of molybdenum and tungsten dioxides, Aust. J. Chem. 48 (1995) 1473. https://doi.org/10.1071/CH9951473.

[23] E. Ahn, T. Min, J. Lee, I. Lee, Y. Kim, H. Jeen, Role of surface oxidation for thickness-driven insulator-to-metal transition in epitaxial MoO_2 films, Appl. Surf. Sci. 459 (2018) 92–97. https://doi.org/10.1016/j.apsusc.2018.07.188.

[24] H.-S. Kim, J.B. Cook, S.H. Tolbert, B. Dunn, The development of pseudocapacitive properties in nanosized-MoO_2, J. Electrochem. Soc. 162 (2015) A5083–A5090. https://doi.org/10.1149/2.0141505jes.